Available online at www.sciencedirect.com
ScienceDirect
Scripta Materialia 60 (2009) 619–622
Scripta MATERIALIA
www.elsevier.com/locate/scriptamat

Strengthening mechanisms in cryomilled ultrafine-grained aluminum alloy at quasi-static and dynamic rates of loading

Buyang Cao,[a,*] Shailendra P. Joshi[b] and K.T. Ramesh[a]

[a] *Mechanical Engineering Department, The Johns Hopkins University, Baltimore, MD 21218, USA*
[b] *Department of Mechanical Engineering, National University of Singapore, Singapore 117576, Singapore*

Received 7 November 2008; revised 5 December 2008; accepted 11 December 2008
Available online 25 December 2008

To achieve lightweight and high-strength materials, Al alloy has been cryomilled and processed to obtain refined microstructures. The microstructure and strengthening mechanisms of the resulting ultrafine-grained material are investigated in this work. Contributions from the several mechanisms (boundary strengthening, solid solution strengthening, precipitate strengthening and dislocation strengthening) are discussed and estimated using simplified models. Comparison with experimental data suggests some directions for materials design.

Keywords: Ultrafine grained microstructure; Dynamic mechanical analysis; Strengthening; Precipitation

Cryomilling has been described in several papers [1–4] and has been shown to be an effective way to refine grain size in order to make strong but lightweight materials. Mechanical tests show that the strength of cryomilled ultrafine-grained (UFG) Al 5083 is improved significantly [3,5] compared to conventional coarse-grained Al 5083. This high strength provides the basis for further processing to make high-strength, lightweight materials with good ductility [6]. Therefore, it is important to understand the fundamental strengthening mechanisms in cryomilled Al 5083. A couple of papers have examined the strengthening mechanisms in similar materials [3,4] at low rates of loading. This work addresses the specific mechanisms active in cryomilled Al 5083 at both quasi-static and dynamic strain rates.

The material investigated here was provided by the University of California, Davis. Commercial Al 5083 powder was cryomilled, cold isostatic pressed and extruded to achieve a UFG structure [4,5,7]. The microstructures of the as-received and post-deformation cryomilled Al 5083 were observed by transmission electron microscopy (TEM) using a Phillips EM420 operated at 120 kV, and by high-resolution TEM using a CM300 operated at 300 kV. The samples were compressed along the extrusion direction both quasi-statically [5,8] and dynamically using a compression Kolsky bar [9]. As a comparison, a conventional commercial coarse-grained Al 5083 material was compressed at similar strain rates [10]. Figure 1 compares the mechanical responses of the UFG samples with the behaviors of coarse-grained samples. The as-received UFG material has a yield strength of approximately 700 MPa at a strain rate of $10^{-3}\,s^{-1}$ [8] and 720 MPa at a strain rate of $10^{-4}\,s^{-1}$ [5]. This negative strain rate sensitivity found in the cryomilled UFG material at low rates (as in the conventional material [10]) is believed to relate to dynamic strain aging [11] and will not be discussed further in this paper. In dynamic tests conducted (on cylindrical samples 4 mm in diameter and 2.4 mm long) in the Kolsky bar with strain rates of 2×10^3 to $6 \times 10^3\,s^{-1}$, the UFG materials show higher flow strengths of 750–780 MPa, which are much higher than the conventional Al 5083 which has strengths of about 320–350 MPa at both quasi-static and dynamic strain rates.

The higher strength in the cryomilled Al 5083 must be understood in terms of the strengthening mechanisms. Therefore, the microstructures of as-received and deformed samples were characterized in terms of several factors: the grain size, solute concentrations, precipitate and dispersoid distributions, and dislocation structures. The microstructure evolution during the cryomilling process is very complex, e.g. the dispersoids interact with grain boundaries and dislocations, and inhibit grain growth; the solution of Mg and Mn affects the

* Corresponding author. E-mail: bcao3@jhu.edu

1359-6462/$ - see front matter © 2008 Acta Materialia Inc. Published by Elsevier Ltd. All rights reserved.
doi:10.1016/j.scriptamat.2008.12.026

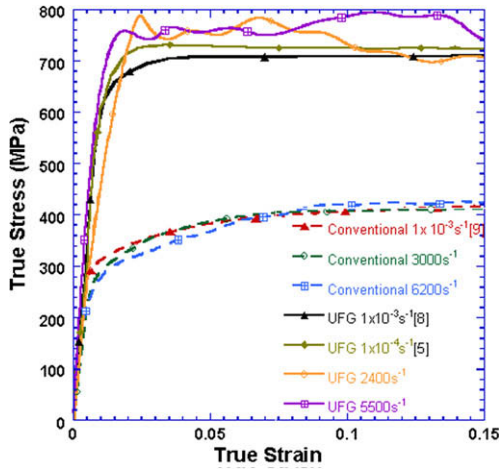

Figure 1. Quasi-static and dynamic responses of cryomilled UFG Al 5083 compared with conventional commercial Al 5083. (UFG 1×10^{-4} and 10^{-3} data from Han et al. [5,8].)

generation of precipitates; and oxides may stabilize the grain boundaries [2]. It is difficult to determine one single constitutive function including all of these factors. In this work, the multiple mechanisms are examined separately, and the strengthening due to each mechanism is calculated using a simplified model that accounts for some (but not all) of the coupling. In general, these multiple strengthening mechanisms may interact with each other. Phenomenological or statistical approaches have been discussed to account for these synergetic effects (e.g. [12]). However, without the knowledge of the specific interactions, we choose a simple linear superposition in order to obtain qualitative estimates of the significance of each mechanism.

As is generally true for UFG materials, the grain size refinement is the fundamental strengthening mechanism. In the cryomilled Al 5083, grains are refined mainly in the milling process, and the grain growth during hot isostatic pressing and extrusion is inhibited by the presence of dispersoids. The material also shows grain anisotropy between extrusion and transverse directions. Based on multiple TEM observations, the linear dimensions of the UFG grains were measured in each direction. The grains were elongated along the extrusion direction with a mean length of 390 nm. In the transverse direction, equiaxed grains were observed with a mean diameter of 150 nm. The Hall–Petch equation estimates the increase of the yield strength due to the refinement of the grains:

$$\Delta\sigma_y = k_y \tilde{d}^{-1/2}, \tag{1}$$

where k_y is the Hall–Petch coefficient and $\tilde{d}$ is the effective grain size, which was calculated by assuming that the grains are cylinders with a volume given by $V = \pi d^2 h/4$ (d being the diameter of the equiaxed grain in the transverse direction, and h being the length of each elongated grain in the extruded direction). The side of a cube of equivalent volume is used to define the effective grain size $\tilde{d} = \sqrt[3]{\pi d^2 h/4}$. This effective grain size $\tilde{d}$ was found to be 190 nm, and this, together with $k_y = 0.28\ \text{MPa}\sqrt{m}$ [2], gives a grain size strengthening increment $\Delta\sigma_y$ of 640 MPa. Note that this k_y is much larger compared to cryomilled pure Al [2]. Later, we briefly elucidate the likely reasons for the high value of k_y for cryomilled Al 5083.

The mechanism of solid solute strengthening is now addressed. Magnesium and manganese are the primary solute atoms in Al 5083 alloy, with 4.4 wt.% Mg and 0.7 wt.% Mn. Ryen et al. [13] examined the effects of magnesium and manganese. The strengthening due to solute atoms can be estimated by [13]:

$$\Delta\sigma_{y\_ss} = KC^n, \tag{2}$$

where C is the concentration of the solute atom and K and n are constants specific to each solute. The maximum possible solute strengthening due to Mg and Mn can be estimated by assuming that all of the Mg and Mn in Al 5083 are dissolved in Al. This maximum strengthening due to 4.4 wt.% Mg solute (as in Al 5083) is 67 MPa [14]. In this material, however, we have found that a large amount of Mg accumulates along the grain boundaries together with a high density of oxygen in the same area. The scanning transmission electron microscopy (STEM) images of Mg and O are presented in Figure 2. Thus the content of the Mg solute in the grain interior has decreased due to precipitation at the boundaries. It is estimated from the STEM information that around 54% of Mg has segregated. Therefore, the actual strengthening due to Mg solute is around 30 MPa. For Mn, according to Ryen et al. [13], the maximum strengthening is 18 MPa in commercially pure Al–Mn with 0.7% Mn.

More than six kinds of dispersoid and precipitate phases [7] are introduced or developed during the processing of cryomilled Al 5083. Our TEM work has found multiple precipitates and dispersoids, which we divide into three types according to their sizes and distribution: (i) Mg along the grain boundary; (ii) Mn-enriched intermetallic phases both inside grains and near grain boundaries; and (iii) nanoparticles (size $\leqslant$ 10 nm, of complex composition [7]) inside grains.

The precipitates in 5xxx Al alloys are complex and their effects on mechanical properties have been described [15,16]. In cryomilled Al 5083, the cryomilling causes the supersaturation of the Mg in Al 5083 and the separation of Mg to grain boundaries [4,17]. Lavernia et al. [2,4] compared the flow stresses of Al–7.5% Mg alloy with varying amounts of solute Mg, and controlled the Mg segregation by heat treatments. They noted that the net flow stresses did not appear to change with Mg content whether the Mg serves as solute atoms or precipitates along grain boundaries. This would imply that

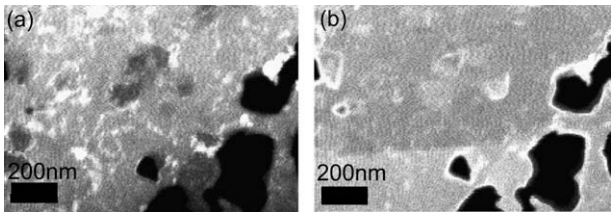

Figure 2. The distribution of (a) Mg and (b) O along grain boundaries. The bright and dark contrast maps the distribution of the specific elements. The brighter an area, the higher the content of the related element.

although the strengthening due to Mg solutes has decreased, the strengthening due to the boundaries has increased, simultaneously resulting in little net change in flow stress. This appears to be just enough to compensate for the loss of Mg as solute atoms (i.e. $K_{Mg}C_{Mg}^{n}+k_{y\text{-}Mg}d^{-1/2}$ should be approximately constant) according to the data of Lavernia et al. [4].

There is evidence that the Hall–Petch coefficient is affected by impurity segregation along grain boundaries [18,19]. Wilson proved experimentally that k_y could depend on solute segregation to the boundaries themselves in steel [18]. Armstrong et al. attribute the larger k_y for mild steel and brass to the segregation effect [19]. A thermodynamically derived model by Li [20] also showed that the obstacle nature of the grain boundary, m (and therefore the Hall–Petch coefficient), should increase with impurity concentration, $\left(\frac{n}{N}\right)$, as $m \sim f\left(\frac{n}{N}\right)$ (n the solute atoms, and N the solvent atoms in the grains). In our case, Mg segregates to the boundaries (Fig. 2), consequently changing k_y. These observations therefore explain why k_y for the cryomilled Al 5083 is apparently much larger [13] than that for cryomilled pure aluminum (0.09 MPa$\sqrt{m}$) [2], and conventional Al 5083 (0.22 MPa$\sqrt{m}$), in which grain boundary segregation of solute atoms is not observed [21].

In Al 5083, the content of manganese is in the range of 0.4–1%. Although the maximum strengthening due to the solute Mn is small (18 MPa as stated above), the precipitate strengthening due to Mn must be considered since its presence is detected in the precipitates by energy-dispersive spectroscopy (EDS) and TEM. The TEM image in Figure 3a shows a commonly observed Mn-enriched intermetallic phase (indicated by the arrows) Al_6Mn, with Fe, Cr and/or Ni substituted for Mn. These precipitates are much harder than the surrounding matrix, showing no change or defects in their structure after dynamic compression. They contribute to the overall strengthening through the particle-size-dependent geometrically necessary dislocations (GNDs) arising from the elastic moduli mismatch and coefficient of thermal expansion (CTE) mismatch between the particles and the matrix [22,23]. The corresponding strength increments are [24]:

$$\Delta\sigma_{GND}^{EM}=\sqrt{3}\eta\mu_m b\sqrt{\rho_{GND}^{EM}} \quad \text{and}$$

$$\Delta\sigma_{GND}^{CTE}=\sqrt{3}\beta\mu_m b\sqrt{\rho_{GND}^{CTE}}, \tag{3}$$

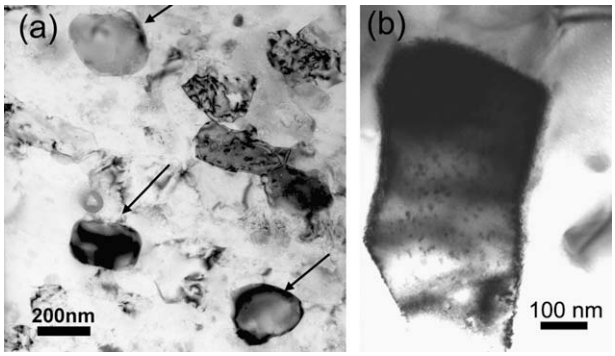

Figure 3. (a) Mn- and Fe-enriched intermetallic phase; (b) nanoparticles inside grains.

where $\rho_{GND}^{EM}=\frac{6f_r\varepsilon}{bd_r}$ and $\rho_{GND}^{CTE}=\frac{12f_r(\Delta\alpha\Delta T)}{bd_r}$ are the GND densities due to the elastic moduli and CTE mismatch, respectively, $\Delta\alpha$ is the CTE mismatch, ε is the misfit strain due to elastic moduli mismatch (assumed the same as the strain due to CTE mismatch $\Delta\alpha\Delta T=0.0065$), b is the magnitude of the Burgers vector, $\mu_m=27$ GPa is the shear modulus of the aluminum matrix, and $\eta=0.5$ and $\beta=0.7$ are geometric constants. The particle size is d_r (~200–300 nm, measured from TEM), the particle volume fraction is f_r (~3.95%, computed assuming that all of the Mn is in the precipitates), and ΔT (~400 K) is the difference between the processing temperature and room temperature. We assume that the particles are incoherent with the matrix, allowing dislocation generation at smaller misfit strains than those required for coherent particles [25]. This strengthening mechanism results in maximum strength increments of $\Delta\sigma_{GND}^{EM}=30$ MPa and $\Delta\sigma_{GND}^{CTE}=60$ MPa, in the limit that all of the Mn is in precipitate form.

The nanoparticles (shown in Fig. 3b) are distributed evenly in the grain interior. The associated Orowan strengthening can be estimated as [26]:

$$\tau_b\cong\frac{\mu_m b}{L-2r}, \tag{4}$$

where L is the distance between the particles and r is the particle size (both measures obtained from the TEM analysis). The dispersoids played a more important role in preventing grain growth than contributing to the strengthening directly via the Orowan mechanism in mechanically alloyed aluminum [27]. We draw similar conclusions here: the compressive strengthening due to these nanoparticles is only around 40 MPa and does not play an important role in overall strength of the cryomilled material.

The final strengthening mechanism considered here is the dislocation strengthening due to prior plastic work. Figure 4a and b shows, respectively, the dislocation structures in the as-received and dynamically deformed samples with a strain rate of 6000 s^{-1}. Even in the as-received samples, there is a high density of dislocations due to previous plastic deformation during processing. The dislocation densities in samples compressed at 6000 s^{-1} are estimated to be ~10^{14}–10^{15} m^{-2} [28,29], and similar densities are apparent in the as-received material. The increase in the shear strength due to dislocations can be estimated by [26]:

$$\Delta\tau=A\mu_m b\sqrt{\rho}, \tag{5}$$

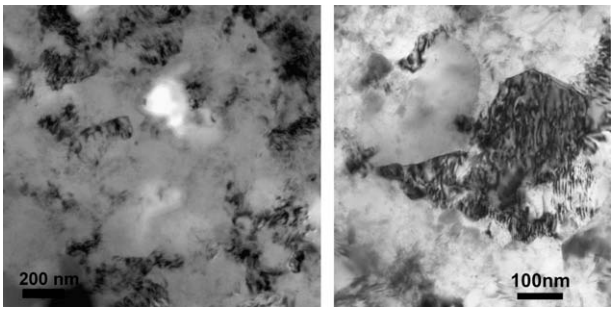

Figure 4. Dislocation structures in cryomilled UFG Al 5083: (a) untested; (b) compressed at a strain rate of ~6000 s^{-1}.

Table 1. Strengthening in cryomilled Al 5083. Minimum and maximum values are given considering the uncertainty in the dislocation density and minimizing the overlap of solute strengthening and precipitate strengthening with respect to Mn content.

Strengthening mechanisms	Strengthening (MPa)	
	Max.	Min.
Grain refinement	640	640
Solid solution		
4.77 wt.% Mg	30	30
0.68 wt.% Mn	0	18
Precipitate		
Nanoparticles	40	0
Intermetallic	90	0
Mg along grain boundary	0	0
Dislocations	85	27
Total	885	715

where A is around 0.2 for face-centered cubic (fcc) materials [26]. The hardening due to dislocation strengthening is thus around 27–85 MPa.

Oxygen and nitrogen are introduced into cryomilled Al alloys during powder processing [2]. These can react with aluminum to form oxides, nitrides and oxynitrides, which can be dispersed in the material, but may be difficult to observe [1–3]. The main function of these dispersoids is stabilizing the grain size through Zener pinning [1,3]. They also contribute to strengthening via the Orowan mechanism [30]. The precise Orowan strengthening due to these is difficult to compute because the dispersoids are so rarely observed given their likely size. A small amount of hydrogen (18–425 ppm) has also been detected in this material [2], which might contribute to strengthening by pinning the dislocations, but this contribution can be ignored compared to strengthening due to other mechanisms.

The multiple strengthening mechanisms that contribute to the higher strength in cryomilled Al 5083 are summarized in Table 1. Minimum and maximum values are given considering the uncertainty in the dislocation density and minimizing the overlap of solute strengthening and precipitate strengthening with respect to Mn content. The contribution from Mg segregation is included in grain refinement strengthening. Compared to the experimental results shown in Figure 1, the total strength from all these mechanisms predicts the minimum strengthening that the material can achieve. The grain size refinement plays the most important role, and hence controlling the grain size is the most effective way to improve strength. Precipitates and solid solution strengthening involve complex mechanisms due to their distributions in the material and contribute more to preventing grain growth than directly to strengthening. Due to the previous heavy plastic deformation during processing, no further work hardening is expected. The mild rate sensitivity observed in the cryomilled material but absent from the conventional coarse-grained material over this range of strain rates is likely a grain size effect [31] that has been previously observed in fcc metals.

Financial support from the Army Research Laboratory, the discussion with Prof. Lavernia's group at the University of California, Davis, and the technical assistance of Dr. Kenneth Livi with the STEM are gratefully acknowledged.

[1] R.J. Perez, B. Huang, E.J. Lavernia, Nanostruct. Mater. 7 (1996) 565.
[2] D.B. Witkin, E.J. Lavernia, Prog. Mater. Sci. 51 (2006) 1.
[3] V.L. Tellkamp, A. Melmed, E.J. Lavernia, Metall. Mater. Trans. A 32 (2001) 2335.
[4] B.Q. Han, Z. Lee, S.R. Nutt, E.J. Lavernia, F.A. Mohamed, Metall. Mater. Trans. A 34 (2003) 603.
[5] B.Q. Han, J.Y. Huang, Y.T. Zhu, E.J. Lavernia, Scripta Mater. 54 (2006) 1175.
[6] B.Q. Han, J.Y. Huang, Y.T. Zhu, E.J. Lavernia, Acta Mater. 54 (2006) 3015.
[7] G. Lucadamo, N.Y.C. Yang, C. San Marchi, E.J. Lavernia, Mater. Sci. Eng. A 430 (2006) 230.
[8] B.Q. Han, Z. Lee, D. Witkin, S. Nutt, E.J. Lavernia, Metall. Mater. Trans. A 36 (2005) 957.
[9] K.T. Ramesh, R.S. Coates, Metall. Mater. Trans. A 23 (1992) 2625.
[10] E.L. Huskins, B. Cao, K.T. Ramesh, in preparation.
[11] G.J. Fan, H. Choo, P.K. Liaw, E.J. Lavernia, Acta Mater. 54 (2006) 1759.
[12] E. Nembach, Acta Metall. Mater. 40 (1992) 3325.
[13] Ø Ryen, O. Nijs, E. Sjölander, B. Holmedal, H. Ekström, E. Nes, Metall. Mater. Trans. A 37 (2006) 1999.
[14] T. Mukai, K. Higashi, S. Tanimura, Mater. Sci. Eng. A 176 (1994) 181.
[15] D.M. Riley, P.G. McCormick, Acta Metall. 25 (1977) 181.
[16] W. Wen, Y. Zhao, J.G. Morris, Mater. Sci. Eng. A 392 (2005) 136.
[17] F. Zhou, R. Rodriguez, E.J. Lavernia, Mater. Sci. Forum 386–388 (2002) 409.
[18] D.V. Wilson, Metal Sci. J. 1 (1967) 40.
[19] R.W. Armstrong, in: A.R. Rosenfield, G.T. Hahn, A.L. BementJr., R.I. Jaffee (Eds.), Dislocation Dynamics, McGraw-Hill, New York, 1967, pp. 293–305.
[20] J.C.M. Li, Trans. Metall. Soc. AIME 227 (1963) 239.
[21] S.P. Joshi, C. Eberl, B. Cao, K.T. Ramesh, K.J. Hemker, Exp. Mech., in press.
[22] M.F. Ashby, Philos. Mag. 21 (1970) 399.
[23] L.H. Dai, Z. Ling, Y.L. Bai, Compos. Sci. Technol. 61 (2001) 1057.
[24] S.P. Joshi, K.T. Ramesh, Scripta Mater. 57 (2007) 877.
[25] M.F. Ashby, L. Johnson, Philos. Mag. 20 (1969) 1009.
[26] T.H. Courtney, Mechanical Behavior of Materials, McGraw-Hill, Singapore, 2000.
[27] J.A. Hawk, P.K. Mirchandani, R.C. Benn, H.G.F. Wilsdort, in: Y.W. Kim, W.M. Griffith (Eds.), Dispersion Strengthened Aluminum Alloys, TMS, Materials Park, OH, 1988, pp. 517–537.
[28] K.T. Park, J.H. Park, Y.S. Lee, W.J. Nam, Mater. Sci. Eng. A 408 (2005) 102.
[29] S.C. Wang, Z. Zhu, M.J. Starink, J. Microsc. 217 (2005) 174.
[30] N. Hansen, Acta Metall. 18 (1970) 137.
[31] Q. Wei, S. Cheng, K.T. Ramesh, E. Ma, Mater. Sci. Eng. A 381 (2004) 71.